HHS Public Access

Author manuscript

Nat Med. Author manuscript; available in PMC 2019 January 02.

Published in final edited form as:

Nat Med. 2018 August ; 24(8): 1121–1131. doi:10.1038/s41591-018-0087-6.

Metformin reverses established lung fibrosis in a bleomycin model

Sunad Rangarajan[1], **Nathaniel B. Bone**[1], **Anna A. Zmijewska**[1], **Shaoning Jiang**[1], **Dae Won Park**[1,3], **Karen Bernard**[1], **Morgan L. Locy**[1], **Saranya Ravi**[2], **Jessy Deshane**[1], **Roslyn B. Mannon**[1], **Edward Abraham**[4], **Victor Darley-Usmar**[2], **Victor J. Thannickal**[1,*], and **Jaroslaw W. Zmijewski**[1,*]

[1]Department of Medicine, University of Alabama at Birmingham, Birmingham, AL 35294-0012, USA

[2]Department of Pathology, University of Alabama at Birmingham, Birmingham, AL 35294-0012, USA

[3]Division of Infectious Diseases, Korea University Ansan Hospital, Ansan 425-707

[4]Office of the Dean, School of Medicine, University of Miami, Miami, FL 33136, USA

Abstract

Fibrosis is a pathological result of a dysfunctional repair response to tissue injury and occurs in a number of organs, including the lungs[1]. Cellular metabolism regulates tissue repair and remodeling responses to injury[2–4]. AMPK is a critical sensor of cellular bioenergetics and controls the switch from anabolic to catabolic metabolism[5]. However, the role of AMPK in fibrosis is not well understood. In this report, we demonstrate that in the humans with idiopathic pulmonary fibrosis (IPF) and in an experimental mouse model of lung fibrosis, AMPK activity is lower in fibrotic regions associated with metabolically active and apoptosis-resistant myofibroblasts. Pharmacological activation of AMPK in myofibroblasts from lungs of humans with IPF display lower fibrotic activity, along with enhanced mitochondrial biogenesis and normalization of sensitivity to apoptosis. In a bleomycin model of lung fibrosis in mice, metformin therapeutically

[*]**Correspondence:** Jaroslaw W. Zmijewski, Ph.D. or Victor J. Thannickal, M.D., Division of Pulmonary Allergy and Critical Care Medicine. Department of Medicine University of Alabama at Birmingham. 901 19th St. South, BMRII 401. Birmingham, AL 35294. Phone: (205) 934-7793. Fax: (205) 934-7437 zmijewsk@uab.edu, vthannickal@uabmc.edu.
[*]V.J.T and J.W.Z contributed equally to the study.

Author contributions

Conception and design: V.J.T and J.W.Z.

Experiments, data analysis and interpretation: Su.R, S.J, D.W.P, N.B.B, K.B, J.D, A.A.Z, R.B.M, M.L.L, Sa.R, E.A., V.D.-U, V.J.T and J.W.Z.

Drafting and revising the manuscript: Su.R, V.J.T and J.W.Z.

Disclosures

All authors declare no conflict of interest.

Life Sciences Reporting Summary

Further information on experimental design and reagents is available in the Life Sciences Reporting Summary.

Data availability

The data that support the findings of this study are available from the corresponding authors upon reasonable request.

accelerates the resolution of well-established fibrosis in an AMPK-dependent manner. These studies implicate deficient AMPK activation in non-resolving, pathologic fibrotic processes, and support a role for metformin (or other AMPK activators) to reverse established fibrosis by facilitating deactivation and apoptosis of myofibroblasts.

Keywords

Lung fibrosis; AMPK; metabolism; mitochondria; bioenergetic reprogramming; extracellular matrix; apoptosis

Pulmonary fibrosis can be the sequelae of lung injury resulting from severe infections, radiation, chemotherapy, environmental exposures or unknown etiologies, as in idiopathic pulmonary fibrosis (IPF). IPF is a progressive, and ultimately fatal, respiratory disorder that affects more than 150,000 patients annually in the United States and over 5 million worldwide[6, 7]. In response to injury, tissue remodeling and formation of fibrotic scars are initiated and perpetuated by biomechanical and biochemical factors, including transforming growth factor beta 1 (TGF-β1) which stimulates anabolic metabolism in activated myofibroblasts[8–11]. Notably, this phenotype is associated with dysfunctional autophagy and acquisition of apoptosis-resistance, events that are implicated in persistence of fibrosis[12–15]. Despite significant progress in the understanding of pathological mechanisms of persistent fibrosis, effective therapeutic interventions have yet to be identified.

AMPK is well-recognized as a cellular bioenergetic sensor and metabolic regulator[5, 16]. Reduced activity of AMPK has been implicated in diabetes mellitus, obesity and aging[17–19], which are known risk factors for development of organ fibrosis[15, 20, 21]. In pre-clinical studies, AMPK activators exert protective effects on lung injury that includes airway remodeling in asthma, with mitigation of the subsequent development of fibrosis[22, 23]. Metformin was recently shown to prevent lung fibrosis *via* NOX4 suppression[24]. Interestingly, AMPK activation may inhibit myofibroblast differentiation by TGF-β1, supporting a preventive role of AMPK in the development of fibrosis[25, 26]; however, whether modulation of this pathway is beneficial in established fibrosis is not known.

Lungs from human subjects with IPF are characterized by architectural tissue remodeling with accumulation of α-smooth muscle actin (α-SMA)-expressing myofibroblasts within fibroblastic foci (Fig. 1a,b and Supplemental Fig. 1a,b). Within these regions of active fibrosis, a significant decrease in AMPK activity, as evidenced by reduced Thr172-AMPK phosphorylation, is observed (Fig. 1a-c and Supplemental Fig. 1c-e). While α-SMA expressing myofibroblasts are largely deficient in AMPK activity, alveolar epithelial cells (AECs) display relatively high levels of AMPK activity in both control and IPF lung tissues (Fig. 1a-c and Supplemental Fig. 2). Next, we examined whether the state of AMPK activity in isolated lung fibroblasts from human subjects with IPF and age-matched control subjects (Supplemental Tables 1 and 2). Despite notable heterogeneity, IPF fibroblasts demonstrate lower levels of AMPK activity (Supplemental Fig. 3a), in association with mTOR activation (evidenced by S6 phosphorylation), HIF-1α accumulation, diminished autophagy (evidenced by LC3BI to LC3BII conversion), and increased lactate production (Supplemental Fig. 3b). The AMP mimetic, AICAR, activates AMPK in a dose-dependent

manner, reduces mTOR-dependent S6 phosphorylation, and induces autophagy, in association with reduced constitutive levels of the extracellular matrix (ECM) proteins, collagen and fibronectin (Fig. 1d,e). Together, these studies indicate that AMPK activation reprograms metabolism in IPF fibroblasts by enhancing autophagy and reducing mTOR activation, while downregulating steady-state levels of ECM proteins.

TGF-β1 is critical mediator of fibrogenic processes in diverse organ systems, including IPF[8]. Previous studies have reported anti-fibrotic effects of metformin in multiple organs, primarily by interfering with TGF-β1 signaling[22, 26–29]. However, whether AMPK activation is capable of deactivating differentiated myofibroblasts and resolving fibrosis is not known. We confirmed that the AMPK activator AICAR prevents collagen type I, fibronectin and α-SMA expression in fibroblasts stimulated with TGF-β1 (Supplemental Fig. 3c,d). In contrast, silencing of AMPK mediates a marked increase in constitutive and TGF-β1-induced expression of fibronectin (Supplemental Fig. 3e). To determine the effects of AMPK activation on differentiated myofibroblasts, cells were treated with AICAR (250 μM) or metformin (500 μM) for 24 hours after TGF-β1 (2.5 ng/ml) stimulation; this resulted in a significant decrease in the steady-state levels of collagen and fibronectin (Fig. 2a,b). Next, we examined if the AMPK-dependent activation of autophagy regulates ECM turnover. The addition of chloroquine, which blocks late autophagy, shows intracellular accumulation of collagen within stabilized autophagosomes (Fig. 2c,d); this suggested the possibility that autophagy controls the turnover of collagen. To test this, we silenced upstream regulators of autophagy, including AMPK, beclin, or LC3B; the effects of AICAR on suppressing steady-state levels of collagen induced by TGF-β1 is lost when autophagy is inhibited (Fig. 2e,f). Notably, prolonged activation of AMPK by AICAR reduces the accumulation of collagen within the extracellular space (Supplemental Fig. 3f).

Loss of AMPK activity may contribute to mitochondrial dysfunction and metabolic reprogramming that regulates myofibroblast differentiation and function[10, 11, 30]. Transmission electron microscopic analysis indicated that IPF myofibroblasts contain fragmented mitochondria, likely due to defective clearance of damaged/dysfunctional mitochondria (Fig. 3a). This is accompanied with enhanced mitochondrial reactive oxygen species formation (data not shown). Bioenergetic analysis revealed that AMPK-deficient fibroblasts have diminished basal oxygen consumption, ATP-linked OCR, maximal respiration, and reduced mitochondrial reserve capacity (Fig. 3b). S555-ULK1 phosphorylation[31], a key regulator of mitophagy, was also diminished in *AMPK*$^{-/-}$ fibroblasts (Fig. 3c). Mitochondria are critical regulators and effectors of programmed cell death[32, 33] and metabolic reprogramming towards aerobic glycolysis has been implicated in cellular resistance to apoptosis in cancer cells[34, 35]. Mechanism(s) of acquired apoptosis resistance in IPF myofibroblasts is not well understood. However, TGF-β1 has been shown to inhibit serum deprivation-induced apoptosis in lung myofibroblasts[36]. Here, we found that AMPK activation is capable of reversing apoptosis resistance in differentiated myofibroblasts (Fig. 3d,e). Additionally, AMPK activation sensitizes TGF-β1-differentiated myofibroblasts to intrinsic apoptosis, in particular induced by antimycin A, a mitochondrial inhibitor of electron transport chain (ETC) complex III (Fig. 3f). This enhanced sensitivity to apoptosis is lost in AMPK silenced fibroblasts (Supplemental Fig. 3g). A possible mechanism by which fibroblasts recovers sensitivity to intrinsic apoptosis may be due to

enhanced mitochondrial biogenesis. We examined if AMPK activation can promote mitochondrial biogenesis in IPF fibroblasts. The AMPK activators, AICAR or metformin, upregulates mitochondrial transcription factor-A (TFAM; a master regulator of mitochondrial biogenesis) and induces expression of the major components of mitochondrial ETC complexes (Fig. 3g). These results suggest that, in addition to regulating ECM homeostasis, AMPK activation upregulates mitochondrial biogenesis and restores myofibroblast sensitivity to intrinsic apoptosis.

The mouse model of bleomycin-induced lung injury, while the most widely utilized for the study of lung fibrosis, is known to resolve over time[15]; however, mechanisms promoting resolution are not well understood. Metformin is a safe and widely used agent for non-insulin-dependent diabetes, and has therapeutic potential to restore glucose and lipid metabolic homeostasis[37, 38]. We explored whether metformin, via AMPK activation, can accelerate resolution of fibrosis in the bleomycin lung fibrosis model. Initial results showed that a single or two doses of metformin (65 mg/kg; i.p.) had little or no effect. However, mice receiving metformin (65 mg/kg; i.p.) every other day for a total of 18 days, starting on day 10 post-bleomycin (1.25 U; i.t.) lung injury (Supplemental Fig. 4a), demonstrate significant reductions in several pro-fibrotic markers, including total lung hydroxyproline and the expression of α-SMA (Supplemental Fig. 4b-d). Histology and immunohistochemistry show diminished amounts of collagen and α-SMA (Supplemental Fig. 4e). Importantly, these effects of metformin are abrogated in mice genetically deficient in AMPKα1 subunit (Supplemental Fig. 4d,f). We also examined the effects of delayed metformin treatment (65 mg/kg; i.p.), *i.e.* 3 weeks after bleomycin injury for up to an additional 5 weeks (Fig. 4a). Metformin promotes fibrosis resolution even after delayed exposure (Fig. 4b-d). Notably, metformin stimulates TFAM and NDFUB8 expression *in vivo*, indicative of enhanced mitochondrial biogenesis, while α-SMA expression is reduced (Fig. 4e). Lung tissues sections revealed a distinct pattern of AMPK activity between normal and fibrotic regions. During the reparative phase of lung injury, AMPK activity is primarily observed in relatively normal-appearing regions of the lung, while regions of active fibrotic remodeling with abundant α-SMA expression are deficient in AMPK activity (Fig. 4f,g and Supplemental Fig. 5a-c), despite similar levels of total amount of AMPK (Supplemental Fig. 6). Reduced AMPK activation was confirmed in lung fibroblasts isolated from lungs of mice with established fibrosis (Supplemental Fig. 5d). These results are concordant with the observation that AMPK activity is markedly diminished in areas of active fibrosis in individuals with IPF (Fig. 1 and Supplemental Fig. 1).

This is the first study, to our knowledge, to demonstrate that the resolution of lung fibrosis can be accelerated with a pharmacological intervention that targets cellular metabolism. We provide mechanistic insights into myofibroblast deactivation, that include enhanced collagen turnover *via* AMPK-dependent activation of autophagy, while mitochondrial biogenesis was associated with a restoration of sensitivity to intrinsic apoptosis. Although metformin may mediate multiple effects, the loss of its protective effect in AMPKα1 deficient mice indicates that the AMPK-autophagy and AMPK-dependent mitochondrial biogenesis are likely critical mechanisms of metformin action. While we show that AMPK activation promotes myofibroblast deactivation/apoptosis, it is possible that AMPK activation in other cell populations, including alveolar epithelial cells and immune cells, may also mediate pro-

resolution and/or anti-fibrotic effects[39, 12, 13]. Additional salutary effects of AMPK activation may involve clearance of apoptotic cells[40], an important step in the resolution of both inflammation and fibrosis. Together, our studies support the concept that AMPK may function as a critical metabolic switch in promoting resolution of established fibrosis by shifting the balance from anabolic to catabolic metabolism. Additionally, we provide proof-of-concept that activation of AMPK by metformin or other pharmacologic agents that activate these pro-resolution pathways may be a useful therapeutic strategy for progressive fibrotic disorders.

Methods

Methods and any associated references are available in the online version of the manuscript.

Online Methods

Human lung tissues

The study protocol was approved by the local ethics committee under University of Alabama at Birmingham Institutional Review Board. Lung sections of either healthy or IPF biopsies were provided by the Airway Tissue Procurement Program Facility at the University of Alabama, Birmingham and the Pulmonary Hypertension Breakthrough Initiative. Lung sections were formalin fixed and paraffin embedded before being cut into 5 μM slices, as previously described[41].

Mice

All experiments were conducted in accordance with protocols approved by the University of Alabama at Birmingham Animal Care and Use Committee. Male mice (C57BL/6), 8 to 10 weeks of age were purchased from the Jackson Laboratory (Bar Harbor, ME, USA). The mice were kept on a 12-hours light-dark cycle with free access to food and water. *AMPKα1*$^{-/-}$ mice were provided by Dr. Benoit Viollet (Université Paris Descartes, France) and Dr. Giri Shailendra Henry Ford Health System, Detroit, USA).

Mouse model for bleomycin-induced lung injury and development of lung fibrosis

For bleomycin administration, mice were anesthetized with isoflurane followed by intratracheal instillation of bleomycin (1.25 U/kg, i.t.) in 60 μl PBS, as previously described[42]. Mice received the first dose of saline (control group) or metformin (65 mg/kg, i.p.) 10 days after bleomycin as described. Saline or metformin (65 mg/kg, i.p.) was then administered every second day for additional 18 days. Additional experiments were designed to measure the effects of delayed metformin administration. In particular, metformin treatment was initiated 3 weeks after exposure to bleomycin. Mice received metformin (every other day) for 5 weeks.

Reagents and antibodies

Recombinant human TGF-β1 was purchased from R&D systems (Minneapolis, MN). Metformin and RPMI 1640, and antimycin A were from Sigma-Aldrich (St. Louis, MO). 5-Aminoimidazole-4-carboxamide-1-β-d-ribofuranoside (AICAR) was purchased from

Toronto Research Chemicals (Toronto, Canada). Bleomycin sulfate, specific siRNA to AMPKα1/2 subunit, scrambled siRNA and Accell culture medium were purchased from Thermo Fisher Scientific (Waltham, MA). In Situ Cell Death Detection Kit (TUNEL assay) was obtained from Roche (Indianapolis, IN). Antibodies to phospho-Thr172 AMPK and cl. PARP were purchased from Cell Signaling Technology (Beverly, MA). For immunohistochemistry, anti phospho-Thr172 AMPK antibody was obtained from Cell Signaling Technology whereas total anti-total AMPKα subunit and anti-T1α IgG were purchased from R&D Systems (Minneapolis, MN). Antibodies to β-actin, fibronectin and α-smooth muscle actin (α-SMA) were obtained from Sigma-Aldrich (St. Louis, MO), whereas anti-GAPDH antibody was from EMD Millipore (Billerica, MA). Anti- human collagen (type I) antibody was purchased from Abcam (Cambridge, MA). Goat anti-rabbit and anti-mouse IgG with horseradish peroxidase (HRP) conjugate were obtained from Bio-Rad (Hercules, CA). Emulsion oil solution containing 4′,6-diamidino-2-phenylindole (DAPI) was from Vector Laboratories (Burlingame, CA) and Hoechst dye were from Life Technologies (Grand Island, NY).

Hydroxyproline content of whole lung

Mouse lung tissues were homogenized using 100 μl water for every 10 mg of tissue. Next, 100 μl HCl (12N) were added per each 100 μl sample of homogenate. Samples in teflon capped vials were then hydrolyzed at 96°C for 48 hours. Next, 10 μl of each sample were transferred to a 96-well plate and evaporated under a vacuum until dry. 100 μl of the chloramine T reagent were added to each sample and standard and incubated at room temperature for 5 minutes. 100 μl of the DMAB reagent were added to each well and incubated for 90 minutes at 60°C. The absorbance was measured (λ = 560 nm) using BioTek ELx800 plate reader. The amount of hydroxyproline in samples was calculated using standard that was prepared accordingly to manufacturer protocol (BioVision, CA).

Lung histology and imaging

Mouse lungs were inflated with 1 ml of 10% paraformaldehyde/PBS solution and embedded in paraffin. 5-μm-thick sections (mouse and human) deparaffinized in serial solutions of Citrisolv (Fisher Scientific, Pittsburgh, PA), isopropyl alcohol, and water, followed by antigen retrieval by steaming in 10 mM citric acid (pH 6.0) for 20 min followed by a 20 min cooling period. The lung sections (mouse or human non-IPF or IPF) were washed with TBST buffer and blocked with 3% BSA for 90 minutes. Next, samples were incubated with anti-phospho-Thr172 AMPK, total AMPK, anti-α-SMA or anti-T1α antibody overnight at 4°C and then secondary FITC or rhodamin-labeled antibody for 60 minutes. Nuclei were stained with DAPI. Fluorescent intensity was measured in randomly chosen area sections of control and IPF lung sections, or sections obtained from experimental group of mice. The levels of fluorescence were quantitated and displayed as two-dimensional scattergrams using HCImage Hamamatsu's image acquisition and analysis software. We also processed paraffin-embedded tissue sections for lung histology and immunohistochemical staining, including H&E, Masson's trichrome or α-SMA staining as previously described[42].

Culture of fibroblast populations

Control (non-IPF) and IPF human lung fibroblasts were provided through the Clinical Core UAB. Human lung diploid (IMR90) fibroblasts were obtained from American Type Culture Collection (ATCC). Cells were cultured in RPMI 1640 medium and DMEM supplemented with 10% heat-inactivated FBS, penicillin (100 U/ml), streptomycin (25 μg/ml) and L-glutamine (1 mM). Cells were maintained at 37°C and 5% CO_2 incubator.

Western Blot analysis

Western Blot analysis were performed as described previously[43]. Briefly, cell lysates or lung homogenates were prepared using lysis buffer containing Tris pH 7.4 (50 mM), NaCl (150 mM), NP-40 (0.5%, vol/vol), EDTA (1 mM), EGTA (1 mM), okadaic acid (1 nM), and protease inhibitors. The protein concentrations in the supernatants were determined using the Bradford reagent (BioRad) with BSA as a standard. After SDS-PAGE, PVDF membranes were probed with specific antibodies as described in the figure legends followed by detection with HRP-conjugated goat anti-rabbit or anti-mouse IgG. Bands were visualized by enhanced chemiluminescence (Super Signal; Pierce Biotechnology, Rockford, IL) and quantified by AlphaEaseFC software (Alpha Innotech, San Leandro, CA).

Extracellular matrix extraction

Extracellular matrix extraction was performed on culture fibroblasts, as described previously[44].

siRNA knockdown of beclin, LC3B and AMPK

Fibroblasts were incubated with specific siRNA (0.1 μM) to AMPKα1/2, beclin or LC3B, as described previously[43]. Briefly, cells (2.5×10^4/well) in 24-well plates were incubated in Accell medium (serum free) containing specific or scrambled siRNA (0.1 μM) for 72 hours. After incubation with siRNA, the cell culture medium was changed to RPMI 1640 medium supplemented and treated as described in figure legends. The sense sequences used for siRNA are as follows: beclin-1: CAGUUUGGCACAAUCAAUA; LC3B: GAAGGCGCUUACAGCUCAA and AMPKα: AUGAUGUCAGAUGGUGAAUUU; non-targeting: UAAGGCUAUGAAGAGAUAC.

Measurement of fibroblast bioenergetics

The bioenergetics was determined using the XF24 analyzer from Seahorse Bioscience, which measures O_2 consumption and proton production (pH) in intact cells, as performed previously[45]. In particular, the O_2 consumption rate (OCR) is correlated with oxidative phosphorylation, and proton production (extracellular acidification rate) can be related to glycolysis. Measurements were performed using 5×10^4/ cells well that were plated on XF24 plates. The plate was then washed with XF assay buffer (DMEM, 5% FBS supplemented with 5.5 mM, D-glucose, 4 mM L-glutamine, and 1 mM pyruvate (pH 7.4) and incubated in XF buffer for 30–60 min before the assay. All results were corrected for cell number in individual wells.

Transmission electron microscopy (TEM)

Lung fibroblasts were fixed in 2.5% glutaraldehyde in 0.05 M cacodylate buffer with 0.1M NaCl, pH 7.5 for 20 minutes at room temperature, as previously described (www.nature.com/protocolexchange/protocols). Transmission electron micrographs and quantitative analyses of morphometric data from TEM images were obtained in collaboration with the High Resolution Image Facility (UAB).

Measurement of fibroblast resistance to apoptosis

For TUNEL assay, cells were culture as indicated in figure legends followed by inclusion of paraformaldehyde and then BrdU assay, accordingly with manufacturer protocol (Roche, Indianapolis, IN). Nuclei were stained with DAPI and images acquired using Leica epifluorescence microscope (Leica Microsystems Inc., Buffalo Grove, IL).

Statistical analysis

Multigroup comparisons were performed using one-way ANOVA with Tukey's post hoc test. Student's *t*-test was used for comparisons between two groups. All tests utilized one-tailed methodology. A P value of less than 0.05 was considered significant. Replicates consist of at least 3 independent experiments. Analyses were performed on SPSS version 16.0 (IBM, Armonk, NY) for Windows (Microsoft Corp., Redmond, WA) and Prism Software (GraphPad Software, San Diego, CA). Image fluorescent analysis, including Parson's correlation was determined using HCImage Hamamatsu's image acquisition and analysis software (Hamamatsu Corporation, Sewickley, PA).

Supplementary Material

Refer to Web version on PubMed Central for supplementary material.

Acknowledgments

We thank Dr. Benoit Viollet (INSERM, Paris, France) and Dr. Giri Shailendra (Henry Ford Health System, Detroit, USA) for providing *AMPK α1/2*$^{-/-}$ MEFs and *AMPKα1*$^{-/-}$ mice.

We thank Dr. Yanping Liu (Medicine, UAB) for technical support. We also thank Dr. Judy Creighton (Anesthesiology, UAB) and Neuroscience Molecular Detection and Stereology Core P30 NS047466 (UAB) for help with lung tissue samples/processing.

Funding

This work was supported in part by National Institutes of Health (NIH), HL107585; Department of Defense, W81XWH-17-1-0577; and Pulmonary, Allergy and Critical Care Medicine (UAB) Translational Program for ARDS grants to Jaroslaw W. Zmijewski.

Victor J. Thannickal was supported by NIH grants, P01 HL114470 and R01 AG046210; and a Department of Veterans Affairs Merit Award I01BX003056.

Sunad Rangarajan was supported by National Institutes of Health K08 (HL135399).

Victor Darley Usmar received support from UAB Nathan Shock Center (P30 AG 050886).

References

1. Wynn TA, Ramalingam TR. Mechanisms of fibrosis: therapeutic translation for fibrotic disease. Nat Med. 2012; 18:1028–1040. [PubMed: 22772564]
2. Lumeng CN, Saltiel AR. Inflammatory links between obesity and metabolic disease. J Clin Invest. 2011; 121:2111–2117. [PubMed: 21633179]
3. O'Neill LA, Hardie DG. Metabolism of inflammation limited by AMPK and pseudo-starvation. Nature. 2013; 493:346–355. [PubMed: 23325217]
4. Eltzschig HK, Eckle T. Ischemia and reperfusion--from mechanism to translation. Nat Med. 2011; 17:1391–1401. [PubMed: 22064429]
5. Hardie DG, Ross FA, Hawley SA. AMPK: a nutrient and energy sensor that maintains energy homeostasis. Nat Rev Mol Cell Biol. 2012; 13:251–262. [PubMed: 22436748]
6. Beers MF, Morrisey EE. The three R's of lung health and disease: repair, remodeling, and regeneration. J Clin Invest. 2011; 121:2065–2073. [PubMed: 21633173]
7. Thannickal VJ, Zhou Y, Gaggar A, Duncan SR. Fibrosis: ultimate and proximate causes. J Clin Invest. 2014; 124:4673–4677. [PubMed: 25365073]
8. Duffield JS, Lupher M, Thannickal VJ, Wynn TA. Host responses in tissue repair and fibrosis. Annual review of pathology. 2013; 8:241–276.
9. Bueno M, et al. PINK1 deficiency impairs mitochondrial homeostasis and promotes lung fibrosis. J Clin Invest. 2014
10. Kobayashi K, et al. Involvement of PARK2-Mediated Mitophagy in Idiopathic Pulmonary Fibrosis Pathogenesis. J Immunol. 2016; 197:504–516. [PubMed: 27279371]
11. Bernard K, et al. Metabolic Reprogramming Is Required for Myofibroblast Contractility and Differentiation. J Biol Chem. 2015; 290:25427–25438. [PubMed: 26318453]
12. Ramos C, et al. Fibroblasts from idiopathic pulmonary fibrosis and normal lungs differ in growth rate, apoptosis, and tissue inhibitor of metalloproteinases expression. Am J Respir Cell Mol Biol. 2001; 24:591–598. [PubMed: 11350829]
13. Romero Y, et al. mTORC1 activation decreases autophagy in aging and idiopathic pulmonary fibrosis and contributes to apoptosis resistance in IPF fibroblasts. Aging Cell. 2016
14. Ashley SL, et al. Targeting Inhibitor of Apoptosis Proteins Protects from Bleomycin-Induced Lung Fibrosis. Am J Respir Cell Mol Biol. 2016; 54:482–492. [PubMed: 26378893]
15. Hecker L, et al. Reversal of persistent fibrosis in aging by targeting Nox4-Nrf2 redox imbalance. Science translational medicine. 2014; 6:231ra247.
16. Inoki K, Kim J, Guan KL. AMPK and mTOR in cellular energy homeostasis and drug targets. Annu Rev Pharmacol Toxicol. 2012; 52:381–400. [PubMed: 22017684]
17. Shaw RJ. Metformin trims fats to restore insulin sensitivity. Nat Med. 2013; 19:1570–1572. [PubMed: 24309653]
18. Riera CE, Dillin A. Can aging be 'drugged'? Nat Med. 2015; 21:1400–1405. [PubMed: 26646496]
19. Finkel T. The metabolic regulation of aging. Nat Med. 2015; 21:1416–1423. [PubMed: 26646498]
20. Burkewitz K, Zhang Y, Mair WB. AMPK at the nexus of energetics and aging. Cell Metab. 2014; 20:10–25. [PubMed: 24726383]
21. Salminen A, Kaarniranta K. AMP-activated protein kinase (AMPK) controls the aging process via an integrated signaling network. Ageing research reviews. 2012; 11:230–241. [PubMed: 22186033]
22. Park CS, et al. Metformin reduces airway inflammation and remodeling via activation of AMP-activated protein kinase. Biochem Pharmacol. 2012; 84:1660–1670. [PubMed: 23041647]
23. Liu Z, et al. AMP-activated protein kinase and Glycogen Synthase Kinase 3beta modulate the severity of sepsis-induced lung injury. Mol Med. 2015
24. Sato N, et al. Metformin attenuates lung fibrosis development via NOX4 suppression. Respiratory research. 2016; 17:107. [PubMed: 27576730]
25. Mishra R, et al. AMP-activated protein kinase inhibits transforming growth factor-beta-induced Smad3-dependent transcription and myofibroblast transdifferentiation. J Biol Chem. 2008; 283:10461–10469. [PubMed: 18250161]

26. Thakur S, et al. Activation of AMP-activated protein kinase prevents TGF-beta1-induced epithelial-mesenchymal transition and myofibroblast activation. Am J Pathol. 2015; 185:2168–2180. [PubMed: 26071397]
27. Lim JY, Oh MA, Kim WH, Sohn HY, Park SI. AMP-activated protein kinase inhibits TGF-beta-induced fibrogenic responses of hepatic stellate cells by targeting transcriptional coactivator p300. J Cell Physiol. 2012; 227:1081–1089. [PubMed: 21567395]
28. Li L, et al. Metformin attenuates gefitinib-induced exacerbation of pulmonary fibrosis by inhibition of TGF-beta signaling pathway. Oncotarget. 2015; 6:43605–43619. [PubMed: 26497205]
29. Park IH, et al. Metformin reduces TGF-beta1-induced extracellular matrix production in nasal polyp-derived fibroblasts. Otolaryngology--head and neck surgery : official journal of American Academy of Otolaryngology-Head and Neck Surgery. 2014; 150:148–153. [PubMed: 24357397]
30. Kottmann RM, et al. Lactic acid is elevated in idiopathic pulmonary fibrosis and induces myofibroblast differentiation via pH-dependent activation of transforming growth factor-beta. Am J Respir Crit Care Med. 2012; 186:740–751. [PubMed: 22923663]
31. Egan DF, et al. Phosphorylation of ULK1 (hATG1) by AMP-activated protein kinase connects energy sensing to mitophagy. Science. 2011; 331:456–461. [PubMed: 21205641]
32. Parsons MJ, Green DR. Mitochondria in cell death. Essays in biochemistry. 2010; 47:99–114. [PubMed: 20533903]
33. Tait SW, Green DR. Mitochondria and cell death: outer membrane permeabilization and beyond. Nat Rev Mol Cell Biol. 2010; 11:621–632. [PubMed: 20683470]
34. Kim JW, Tchernyshyov I, Semenza GL, Dang CV. HIF-1-mediated expression of pyruvate dehydrogenase kinase: a metabolic switch required for cellular adaptation to hypoxia. Cell Metab. 2006; 3:177–185. [PubMed: 16517405]
35. Spoden GA, et al. Pyruvate kinase isoenzyme M2 is a glycolytic sensor differentially regulating cell proliferation, cell size and apoptotic cell death dependent on glucose supply. Exp Cell Res. 2009; 315:2765–2774. [PubMed: 19563799]
36. Horowitz JC, et al. Activation of the pro-survival phosphatidylinositol 3-kinase/AKT pathway by transforming growth factor-beta1 in mesenchymal cells is mediated by p38 MAPK-dependent induction of an autocrine growth factor. J Biol Chem. 2004; 279:1359–1367. [PubMed: 14576166]
37. Foretz M, Guigas B, Bertrand L, Pollak M, Viollet B. Metformin: from mechanisms of action to therapies. Cell Metab. 2014; 20:953–966. [PubMed: 25456737]
38. Knowler WC, et al. Reduction in the incidence of type 2 diabetes with lifestyle intervention or metformin. N Engl J Med. 2002; 346:393–403. [PubMed: 11832527]
39. Yu G, et al. Thyroid hormone inhibits lung fibrosis in mice by improving epithelial mitochondrial function. Nat Med. 2018; 24:39–49. [PubMed: 29200204]
40. Jiang S, et al. Mitochondria and AMP-activated protein kinase-dependent mechanism of efferocytosis. J Biol Chem. 2013; 288:26013–26026. [PubMed: 23897815]
41. Jian MY, Alexeyev MF, Wolkowicz PE, Zmijewski JW, Creighton JR. Metformin-stimulated AMPK-alpha1 promotes microvascular repair in acute lung injury. Am J Physiol Lung Cell Mol Physiol. 2013; 305:L844–855. [PubMed: 24097562]
42. Hecker L, et al. NADPH oxidase-4 mediates myofibroblast activation and fibrogenic responses to lung injury. Nat Med. 2009; 15:1077–1081. [PubMed: 19701206]
43. Jiang S, et al. Human Resistin Promotes Neutrophil Proinflammatory Activation and Neutrophil Extracellular Trap Formation and Increases Severity of Acute Lung Injury. J Immunol. 2014
44. Franco-Barraza J, Beacham DA, Amatangelo MD, Cukierman E. Preparation of Extracellular Matrices Produced by Cultured and Primary Fibroblasts. Current protocols in cell biology. 2016; 71:10 19 11–10 19 34. [PubMed: 27245425]
45. Hill BG, et al. Integration of cellular bioenergetics with mitochondrial quality control and autophagy. Biol Chem. 2012; 393:1485–1512. [PubMed: 23092819]

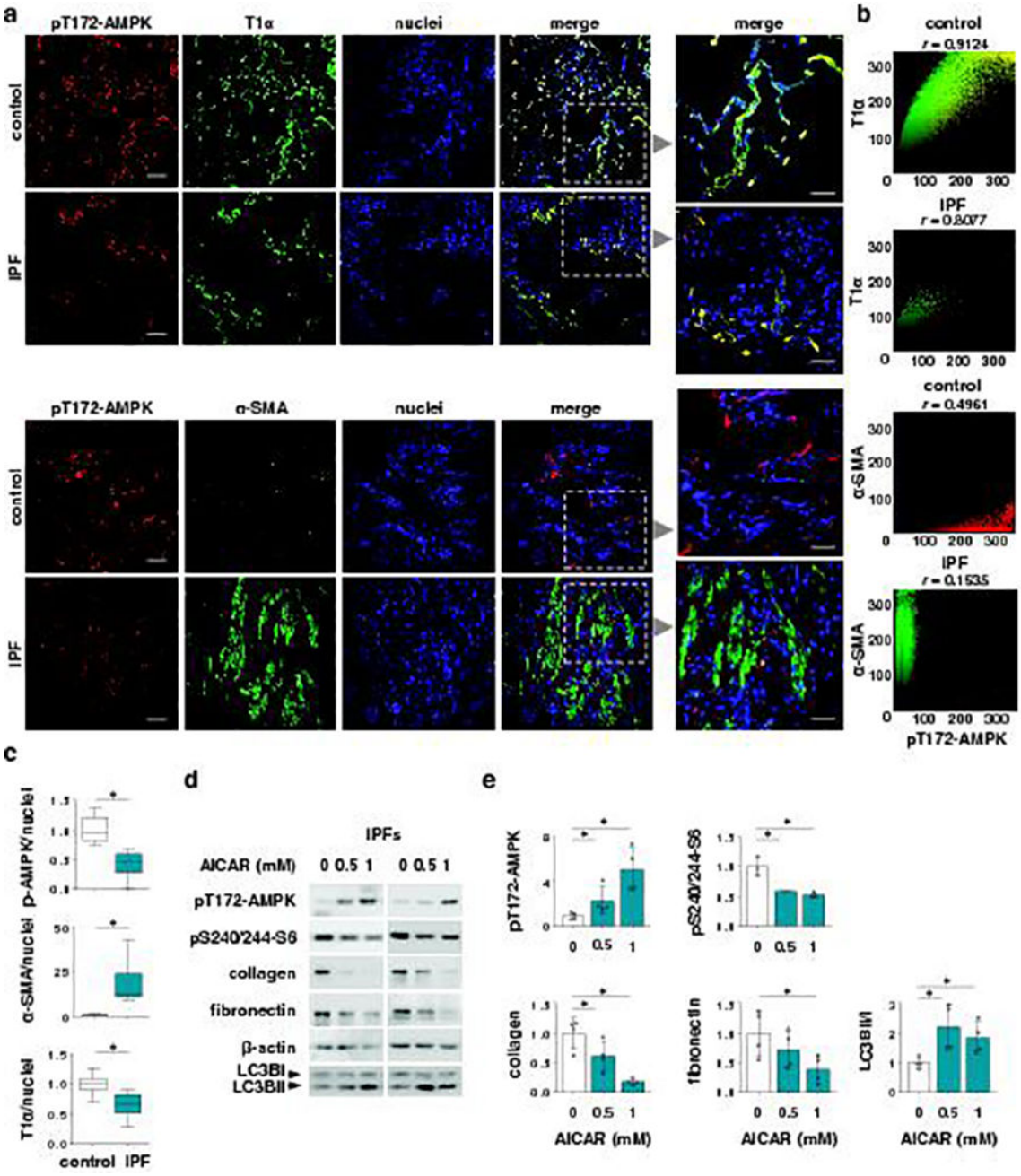

Figure 1.

Distinct patterns of AMPK activity in lung epithelial cells and myofibroblasts of human individuals with IPF. (**a**) Representative images show pT172-AMPK (red), epithelial marker T1α (green), α-SMA (green) and nuclei (blue) in lung sections of control and subjects with IPF. Scale bar, 100 μm. Right panels display magnified areas from images indicated by dashed boxes. Scale bar, 30 μm. (**b**) Scattergrams indicate fluorescence intensity and Pearson's correlation (*r*) in images display in **a**. (**c**) The ratio of pT172-AMPK, T1α or α-SMA to nuclei fluorescence intensity. Means ± SD; $n = 9$ (control), $n = 9$ (IPF) for both pT172-AMPK and α-SMA; $n = 8$ (control), $n = 6$ (IPF) for T1α. *$P < 0.05$ (Student's *t*-

test). (**d**) Representative western blots and quantitative analysis show the amounts of pT172-AMPK, pS240/244-S6 kinase, collagen type I, fibronectin, LC3BI/II and β-actin in IPF fibroblasts stimulated with AICAR (24 h). LC3II/I ratio was obtained from cells treated with AICAR and chloroquine. Means ± SD, $n = 3$ or $n = 4$. $^{*}P < 0.05$ (ANOVA).

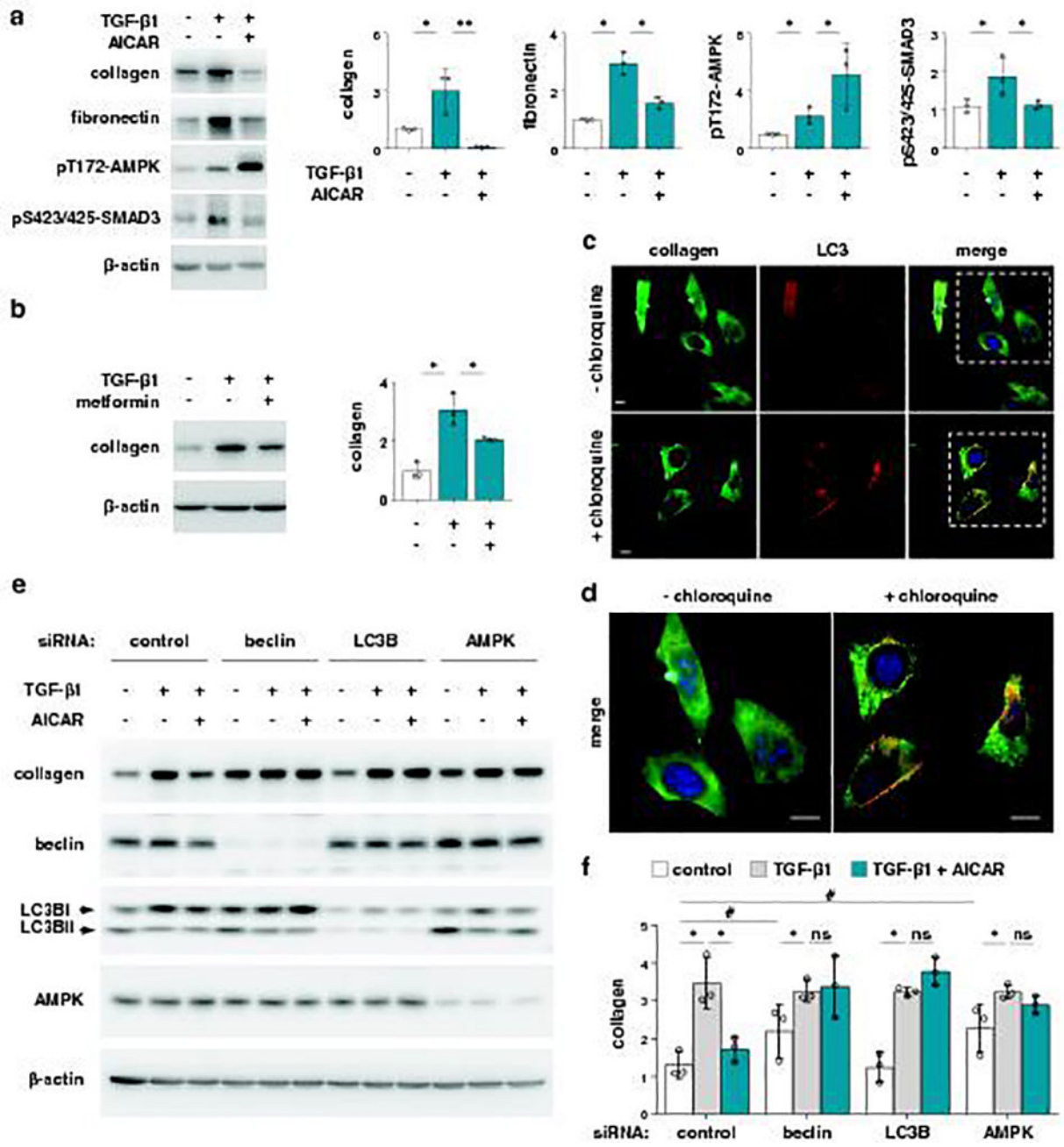

Figure 2.

AMPK activation reduces the levels of ECM proteins in TGF-β1-treated fibroblasts. (**a**) Representative western blots show collagen, fibronectin, pT172-AMPK, pS423/425-SMAD3 and β-actin in human lung fibroblasts treated with TGF-β1 for 24 hours, followed by AICAR for an additional 24 hours. Means ± SD, $n = 3$. $^{*}P < 0.05$ (ANOVA). (**b**) Levels of collagen decrease in fibroblasts treated with metformin- (0 or 1 mM; 24 hours) in TGF-β1-differentiated myofibroblasts. Representative immunoblots are shown. Means ± SD, $n = 3$. $^{*}P < 0.05$ (ANOVA). (**c,d**) Representative images of collagen and LC3 indicate fluorescent staining in control and chloroquine-treated MEFs. Collagen (green), LC3 (red), nuclei

(blue). Scale bar, 25 μM. (**d**) High magnification areas are selected by dashed boxes depicted in **c**. Scale bar, 10 μM. (**e**) Representative western blots show the levels of collagen accumulation in control (scrambled siRNA) and human lung fibroblasts with siRNA-mediated silencing of beclin, LC3B or AMPK. Cells were treated TGF-β1 for 24 hours and then AICAR for an additional 24 hours. (**f**) Optical band densitometry of immunoblots in **e**. Means ± SD, $n = 3$. $^{*}P < 0.05$, ns-not significant (ANOVA). $^{\#}P < 0.05$ (Student's *t*-test).

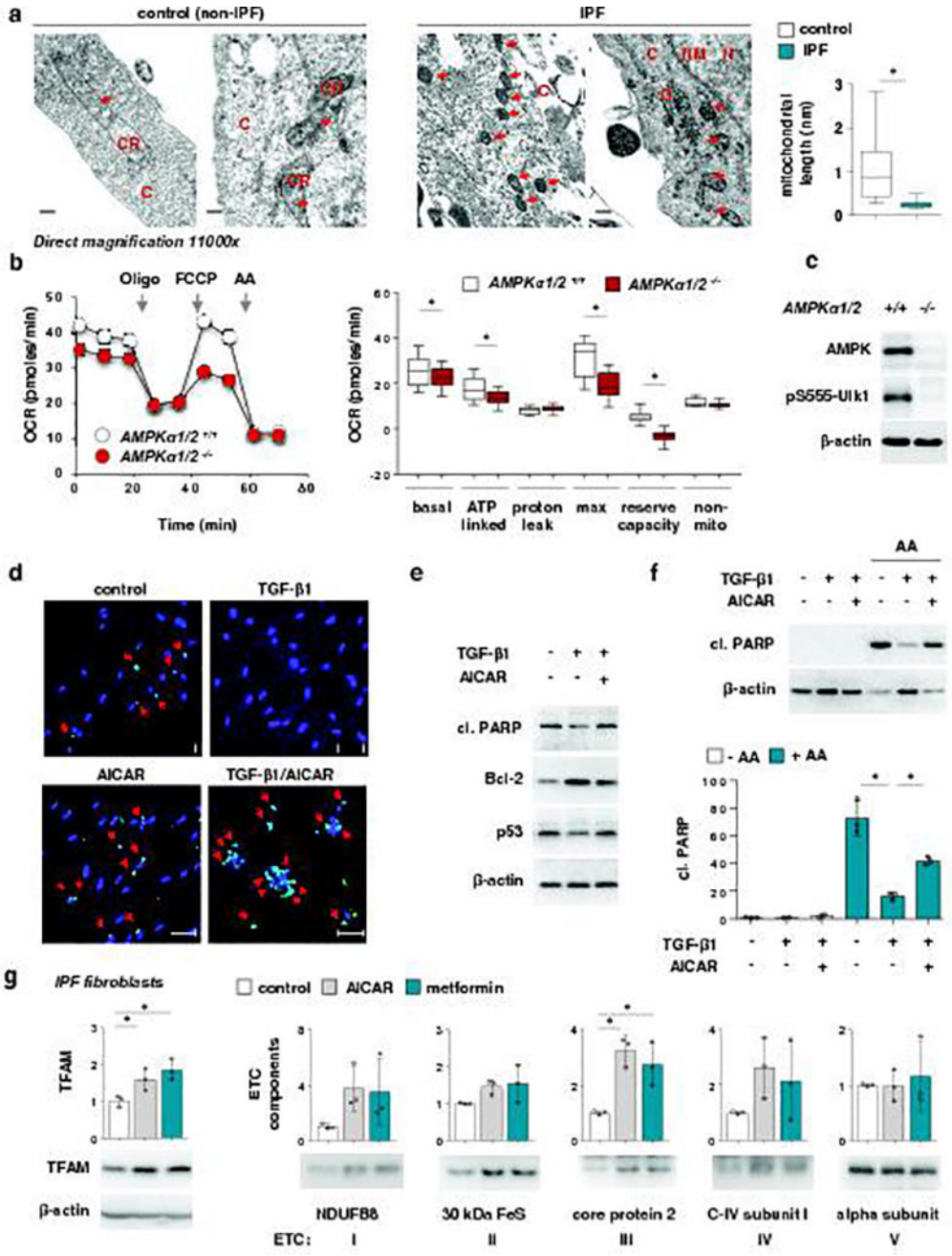

Figure 3.

Effects of AMPK activation on mitochondrial bioenergetics and TGF-β1-mediated resistance to apoptosis in lung fibroblasts. (**a**) Representative transmission electron micrographs show mitochondrial size in cross-section of fibroblasts from control and subjects with IPF. Arrows (mitochondria), CR (cristae), C (cytoplasm), G (golgi). Scale bar, 200 nm. Means ± SEM, $n = 21$ (control), $n = 37$ (IPF) of mitochondria morphometric analysis. $^*P < 0.05$ (Student's *t*-test). (**b**) Representative OCR tracing (left) and bioenergetic indices (right) from wild-type and *AMPKα1/2*$^{-/-}$ MEFs. Means ± SD, $n = 5$. $^*P < 0.05$ (Student's *t*-test). (**c**) Representative western blots of 555-ULK1 phosphorylation in wild-

type and AMPK-deficient MEFs. (**d**) Representative fluorescent staining images of TUNEL (green) and nuclei (blue) in human lung fibroblasts treated with TGF-β1 for 24 hours, followed by AICAR for an additional 7 days. Red arrows indicate TUNEL positive cells. Scale bar, 50 μm. (**e**) Representative immunoblots of cleaved PARP, Bcl2, p53, and β-actin from fibroblasts treated as indicated in **d**. (**f**) Representative immunoblots and quantitative analysis of cleaved PARP in human lung fibroblasts treated with TGF-β1 for 24 hours, followed by AICAR (72 hours), and then antimycin A (AA; 16 hours). Means ± SD, $n = 3$. $^*P < 0.05$ (ANOVA). (**g**) Representative immunoblots of TFAM and components of the ETC complexes in human lung fibroblasts treated with AICAR or metformin for 72 hours. Means ± SD, $n = 3$. $^*P < 0.05$ (ANOVA).

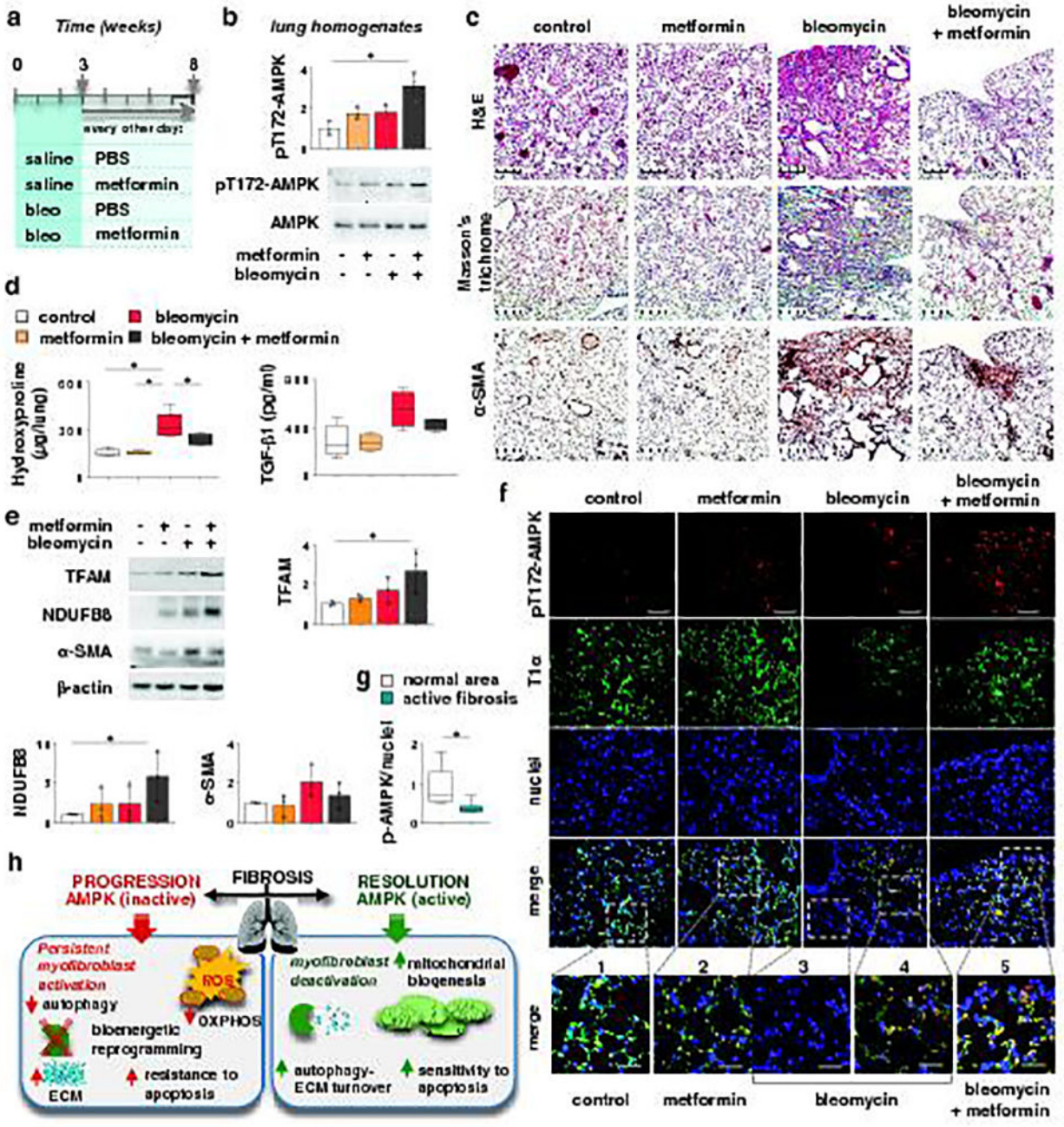

Figure 4.

Metformin accelerates resolution of bleomycin-induced lung fibrosis. Panel (**a**) outlines the design of therapeutic dosing of metformin in mice with established fibrosis following bleomycin-induced lung injury. (**b**) Representative western blots indicate the amounts of pT172-AMPK and total AMPK in lung homogenates from mice treated as depicted in **a**. Means ± SD, $n = 3$. $^*P < 0.05$ (ANOVA). (**c**) Representative images show H&E, Masson's trichrome and α-SMA staining of lung sections from indicated groups of mice. Scale bar, 100 μm. (**d**) Quantitative analysis of hydroxyproline and TGF-β1 in lung homogenates from groups of mice depicted in **a**. Means ± SD, $n = 5$. $^*P < 0.05$ (ANOVA). (**e**) Representative

immunoblots of TFAM, NDUFB8 and α-SMA in whole lung homogenates of mice as indicated. Means ± SD, $n = 3$. *$P < 0.05$ (ANOVA). (**f**) Representative fluorescence images of pT172-AMPK and T1α in lung sections of mice treated, as depicted in **a**. pT172-AMPK (red), type I alveolar epithelial cell marker T1α (green), nuclei (blue). Scale bar, 50 μm. Lower panel shows higher magnification images of areas marked by square boxes (dash lines). Scale bar, 10 μm. (**g**) Quantitative analysis of pT172-AMPK/nuclei fluorescence ratio from normal and fibrotic areas of bleomycin-injured mice. Means ± SD, 3 mice per group, $n = 9$ normal areas, $n = 9$ active fibrosis. *$P < 0.05$ (Student's *t*-test). (**h**) Schematic diagram of the proposed mechanisms for fibrosis resolution induced by AMPK activation. Left panel: loss of AMPK activity promotes persistent myofibroblast activation by deficient autophagy, ECM accumulation, mitochondrial dysfunction and acquired apoptosis resistance. Right panel: AMPK activation stimulates autophagy and facilitates ECM turnover, while inducing mitochondrial biogenesis, thus restoring sensitivity to apoptosis and promoting fibrosis resolution.